

Long-range correlations with finite-size effects from a superposition of uncorrelated pulses with power-law distributed durations

M. A. Korzeniowska^{1,*} and O. E. Garcia^{1,†}

¹*Department of Physics and Technology, UiT The Arctic University of Norway, N-9037 Tromsø, Norway.*

(Dated: March 3, 2025)

Long-range correlations manifested as power spectral density scaling $1/f^\beta$ for frequency f and a range of exponents β are investigated for a superposition of uncorrelated pulses with distributed durations τ . Closed-form expressions for the frequency power spectral density are derived for a one-sided exponential pulse function and several variants of bounded and unbounded power-law distributions of pulse durations $P_\tau(\tau) \sim 1/\tau^\alpha$ with abrupt and smooth cutoffs. The asymptotic scaling relation $\beta = 3 - \alpha$ is demonstrated for $1 < \alpha < 3$ in the limit of an infinitely broad distribution $P_\tau(\tau)$. Logarithmic corrections to the frequency scaling are exposed at the boundaries of the long-range dependence regime, $\beta = 0$ and $\beta = 2$. Analytically demonstrated finite-size effects associated with distribution truncations are shown to reduce the frequency ranges of scale invariance by several decades. The regimes of validity of the $\beta = 3 - \alpha$ relation are clarified.

I. INTRODUCTION

Coherent propagating structures, such as solar phenomena and turbulent flows, are robust examples of naturally occurring scale invariance, long-range correlations and $1/f$ noise [1–9]. Phenomenological modelling of the self-similarity characteristics of fluctuating systems has canonically been done using stochastic processes describing a superposition of uncorrelated pulses [10–13]. These models are highly parametrizable, and spectral scale invariance has been demonstrated for pulses with a power-law shape [11], as well as for distributed inter-event times [14–17], relaxation rates [18], and pulse durations [19, 20]. Recently, a power spectral density scaling as $1/f$ at low frequencies has been shown to result from a sequence of nonoverlapping rectangular pulses with a power law distribution of durations or waiting times [21].

In the highly cited paper by van der Ziel [19], the spectral density of semi-conductor noise $X(t)$ with a probability density of event durations $P_\tau(\tau)$ is constructed as a weighted sum of individual spectral densities, each corresponding to a signal with a single relaxation time,

$$4\langle X(t)^2 \rangle \int_0^\infty d\tau \tau P_\tau(\tau)/(1 + \tau^2 \omega^2), \quad (1)$$

where $\omega = 2\pi f$ is the angular frequency, and the Lorentzian term $(1 + \tau^2 \omega^2)^{-1}$ corresponds to the spectral density of a one-sided exponential pulse function. Importantly, Eq. (1) does not reflect the dynamics of a superposition of uncorrelated pulses with durations distributed continuously over a wide range. In such a process the overlapping long-lasting events instigate internal long-range correlations resulting in algebraic tails of the auto-correlation function. As remarked by Butz [20], the auto-correlation function is then itself τ -dependent, and hence the term $\langle X(t)^2 \rangle$ should be included in the integration, yielding a spectrum proportional to

$$\int_0^\infty d\tau \tau^2 P_\tau(\tau)/(1 + \tau^2 \omega^2). \quad (2)$$

For $P_\tau \sim 1/\tau^\alpha$, Eqs. (1) and (2) indicate different scaling signatures of the frequency power spectral density: $1/\omega^{2-\alpha}$ and $1/\omega^{3-\alpha}$, respectively. Obtaining $1/f$ noise thus calls for $P_\tau \sim 1/\tau$ according to Eq. (1), and $P_\tau \sim 1/\tau^2$ according to Eq. (2). An empirical $1/f$ -like scaling has been demonstrated for an aggregation of random telegraph noise oscillators with individual Lorentzian characteristics [22], speaking to van der Ziel's Eq. (1). Such an aggregate is, however, distinct from a single process consisting of superposed, uncorrelated pulses with distributed durations, whose power spectral density was shown by Butz to follow Eq. (2).

The literature reflects the lack of clarity and discernment on the matter. In Ref. 23, the $1/\omega^{3-\alpha}$ scaling is explicitly acknowledged alongside the derivation of Eq. (1) and a discussion of the resulting $1/\omega^{2-\alpha}$ scaling. The ambiguity is furthered by yet another variant of the spectral density, plausibly dating back to Bernamont [24],

$$\int_{\tau_\downarrow}^{\tau_\uparrow} d\tau P_\tau(\tau)/(1 + \tau^2 \omega^2), \quad (3)$$

where τ_\downarrow and τ_\uparrow are, respectively, the minimum and maximum pulse durations. Equation (3) is mentioned in Refs. 25 and 26 as a substantiation of $1/f$ noise originating from $P_\tau \sim 1/\tau$. We remark that integrating Eq. (3) with $P_\tau = 1/\tau$ yields a logarithmic expression, $\ln[\tau_\uparrow^2(1 + \tau_\downarrow^2 \omega^2)/(\tau_\downarrow^2(1 + \tau_\uparrow^2 \omega^2))] \approx 1/\omega$, which does not display the $1/\omega$ signature even in the limit of an infinitely wide distribution. A uniform P_τ is required for obtaining the $1/\omega$ scaling from Eq. (3).

The main objective of this paper is to present a comprehensive and systematic overview over the scaling characteristics of the frequency power spectral density of a Poisson process with distributed pulse durations, extending the original work by Butz [20] and Milotti [18]. Our analysis includes a derivation of a general integral expression for the power spectral density, followed by closed-form expressions obtained for a one-sided exponential pulse function and several power-law pulse duration distributions with various truncations. The $1/\omega^{3-\alpha}$ scaling of the power spectral density is demonstrated explicitly in the limit of an infinitely broad distribution of durations $P_\tau(\tau) \sim 1/\tau^\alpha$ for $1 < \alpha < 3$, with logarithmic corrections to the frequency scaling exposed for

* magdalena.a.korzeniowska@uit.no

† odd.erik.garcia@uit.no

$\alpha = 1$ and $\alpha = 3$. The emergence of the $1/\omega^{3-\alpha}$ scaling for bounded regions of scale invariance is confirmed by the compensated spectra of the analytical expressions as well as from realizations of the process. This also exposes the finite-size effects associated with the truncation of the underlying pulse duration distributions. It is also demonstrated that for propagating fixed-size pulses observed from a single location, the $P_\tau(\tau) \sim 1/\tau^2$ distribution of their durations is equivalent to a uniform distribution of their velocities, removing the requirement of power-law input for obtaining a $1/f$ noise signature.

This paper is organized as follows. In Sec. II we present the stochastic process describing fluctuations in physical systems as a superposition of uncorrelated pulses. General expressions are derived for the auto-correlation function and the frequency power spectral density for a distribution of pulse durations. Power-law distributions with various support truncations are defined in Sec. III, with complementary definitions presented in Appendix B. Power-law distributed pulse durations are motivated in Appendix A, where for an advection equation we demonstrate that the probability density of pulse durations is characterized by power-law scalings when the corresponding pulse propagation velocities follow a uniform or a Gamma distribution. In Sec. IV we discuss the infinite variance of pulse durations as a prerequisite for long-range correlations, and we establish a relation between the scaling of the frequency power spectral density and the scaling of the underlying distribution of pulse durations. Closed-form power spectral density expressions demonstrating scale invariance and logarithmic corrections to the frequency scaling are derived in Sec. V, with complementary derivations presented in Appendix B. A discussion of the results and conclusions follow in Secs. VI and VII, respectively.

II. STOCHASTIC MODEL

In this section we outline the stochastic process describing fluctuations due to a super-position of uncorrelated pulses with a distribution of durations. General expressions for the two lowest-order moments, the auto-correlation function and the power spectral density are derived. Considering a normalized random variable, a general expression for the dimensionless power spectral density is obtained.

A. Super-position of uncorrelated pulses

Consider a stochastic process given by a superposition of K uncorrelated pulses distributed uniformly in a time interval of duration T [27],

$$\Phi_K(t) = \sum_{k=1}^{K(T)} A_k \phi\left(\frac{t - u_k}{s_k}\right). \quad (4)$$

Each pulse indexed by k is characterized by an amplitude A_k , a duration s_k , and an arrival time u_k , the latter following a uniform probability density, $P_u = 1/T$. The pulse function $\phi(\theta)$ is normalized such that $\int_{-\infty}^{\infty} d\theta |\phi(\theta)| = 1$. The total number

of pulses K arriving in the interval of duration T is a random variable distributed according to a Poisson distribution,

$$P_K(K; T) = \frac{1}{K!} \left(\frac{T}{\langle w \rangle}\right)^K \exp\left(-\frac{T}{\langle w \rangle}\right), \quad (5)$$

where $\langle w \rangle$ is the average pulse waiting time. In a Poisson process, the waiting times between consecutive pulses are exponentially distributed. The pulse durations s_k are assumed to be distributed randomly with probability density $P_s(s)$, and an average pulse duration $\langle s \rangle = \int_0^\infty ds s P_s(s)$. Each of the pulse parameters A , u and s are assumed to be independent and identically distributed.

Given the distribution of pulse amplitudes $P_A(A)$ with a finite mean $\langle A \rangle$ and variance $\langle A^2 \rangle$, the moments and the auto-correlation function of the process defined by Eq. (4) with exactly K pulses are calculated by averaging over all random variables according to Campbell's theorem [28, 29]. Subsequently, averaging over the randomly distributed number of pulses K yields the corresponding expressions for the stationary process [27].

B. Mean and variance

For uniformly distributed pulse arrival times, the conditional mean value of the process with exactly K pulses is given by [27]

$$\langle \Phi_K \rangle = \langle s \rangle \langle A \rangle I_1 K / T, \quad (6)$$

where I_n is the integral of the n 'th power of the pulse function defined for positive integers n as

$$I_n = \int_{-\infty}^{\infty} d\theta [\phi(\theta)]^n. \quad (7)$$

With $K(T)$ following a Poisson distribution, the average number of pulses in an interval of duration T is given by $\langle K \rangle = T/\langle w \rangle$. The mean value of the stationary process is then given by

$$\langle \Phi \rangle = \gamma I_1 \langle A \rangle, \quad (8)$$

where $\gamma = \langle s \rangle / \langle w \rangle$ is the intermittency parameter determining the degree of pulse overlap [30].

The second order moment is calculated in a similar manner, averaging over the square of the random variable $\langle \Phi_K^2 \rangle$. The variance of the process then follows as [27]

$$\langle \Phi^2 \rangle = \langle \Phi \rangle^2 + \Phi_{\text{rms}}^2, \quad (9)$$

where the standard deviation is given by

$$\Phi_{\text{rms}}^2 = \gamma I_2 \langle A^2 \rangle. \quad (10)$$

The absolute level of fluctuations is thus proportional to the degree of pulse overlap described by the parameter γ . Long pulse durations and short waiting times both contribute to the increase in the value of γ and the mean value of the process

given by Eq. (8). Conversely, the relative level of fluctuations of the process with non-zero mean $\langle \Phi \rangle$ is described by

$$\frac{\Phi_{\text{rms}}^2}{\langle \Phi^2 \rangle} = \frac{1}{\gamma} \frac{I_2}{I_1^2} \frac{\langle A^2 \rangle}{\langle A \rangle^2}, \quad (11)$$

which is large when there is a clear separation of pulses with relatively short durations, corresponding to $\gamma \ll 1$. The moments and the characteristic function of the process given by Eq. (4) are independent of the distribution of pulse durations [27].

C. Auto-correlation function

The auto-correlation function of the process $\Phi_K(t)$ for a time lag r is calculated as

$$R_{\Phi_K}(r) = \langle \Phi_K(t) \Phi_K(t+r) \rangle. \quad (12)$$

For a normalized, non-negative pulse function $\phi(\theta)$, averaging over the randomly distributed number of pulses K gives the auto-correlation function for the stationary process [27],

$$R_{\Phi}(r) = \langle \Phi \rangle^2 + \Phi_{\text{rms}}^2 \frac{1}{\langle s \rangle} \int_0^\infty ds s P_s(s) \rho_\phi(r/s), \quad (13)$$

where

$$\rho_\phi(\theta) = \frac{1}{I_2} \int_{-\infty}^\infty d\chi \phi(\chi) \phi(\chi + \theta) \quad (14)$$

is a normalized auto-correlation function of the pulse function.

D. Power spectral density

The power spectral density is given by the Fourier transform of the auto-correlation function in Eq. (13) [27],

$$\begin{aligned} S_{\Phi}(o) &= \int_{-\infty}^\infty dr R_{\Phi}(r) \exp(-ior) \\ &= 2\pi \langle \Phi \rangle^2 \delta(o) + \Phi_{\text{rms}}^2 \frac{1}{\langle s \rangle} \int_0^\infty ds s^2 P_s(s) \varrho_\phi(so), \end{aligned} \quad (15)$$

where $o = 2\pi f$ is the dimensional angular frequency and

$$\varrho_\phi(\vartheta) = \int_{-\infty}^\infty d\theta \rho_\phi(\theta) \exp(-i\vartheta\theta) = \frac{1}{I_2} |\varphi|^2(\vartheta) \quad (16)$$

is the Fourier transform of the normalized auto-correlation of the pulse function given by Eq. (14) and

$$\varphi(\vartheta) = \int_{-\infty}^\infty d\theta \phi(\theta) \exp(-i\vartheta\theta) \quad (17)$$

is the Fourier transform of the pulse function $\phi(\theta)$. The power spectral density given by Eq. (15) is independent of the distribution of pulse amplitudes $P_A(A)$. It is derived for uniformly distributed pulse arrival times, and under the assumption that the two lowest-order moments of the process are finite.

E. Normalization

Consider a rescaled random variable with zero mean and unit standard deviation,

$$\tilde{\Phi} = \frac{\Phi - \langle \Phi \rangle}{\Phi_{\text{rms}}}. \quad (18)$$

The auto-correlation function for the normalized process follows as

$$R_{\tilde{\Phi}}(r) = \frac{1}{\langle s \rangle} \int_0^\infty ds s P_s(s) \rho_\phi(r/s), \quad (19)$$

and the power spectral density, given by the Fourier transform of Eq. (19), becomes

$$S_{\tilde{\Phi}}(o) = \frac{1}{\langle s \rangle} \int_0^\infty ds s^2 P_s(s) \varrho_\phi(so). \quad (20)$$

It should be noted that for the normalized variable, the auto-correlation function and the power spectral density are independent of the intermittency parameter γ . They are defined in terms of the distribution of pulse durations $P_s(s)$ and the transformations of the pulse function, $\rho_\phi(\theta)$ and $\varrho_\phi(\vartheta)$, given respectively by Eqs. (14) and (16).

Normalizing s and o by the mean value $\langle s \rangle$, the dimensionless pulse duration and the angular frequency are introduced respectively as

$$\tau = s/\langle s \rangle, \quad (21a)$$

$$\omega = o/\langle s \rangle. \quad (21b)$$

The normalized probability density function of the dimensionless pulse durations is then given by

$$P_\tau(\tau) = P_s(s/\langle s \rangle) = \langle s \rangle P_s(s), \quad (22)$$

and the power spectral density in Eq. (20) becomes

$$S_{\tilde{\Phi}}(\omega/\langle s \rangle) = \langle s \rangle \int_0^\infty d\tau \tau^2 P_\tau(\tau) \varrho_\phi(\tau\omega). \quad (23)$$

The dimensionless power spectral density defined as $\Omega_{\tilde{\Phi}}(\omega) = S_{\tilde{\Phi}}(\omega/\langle s \rangle)/\langle s \rangle$ then follows as

$$\Omega_{\tilde{\Phi}}(\omega) = \int_0^\infty d\tau \tau^2 P_\tau(\tau) \varrho_\phi(\tau\omega), \quad (24)$$

for a distribution of pulse durations $P_\tau(\tau)$. In the following, only the dimensionless power spectral density form in Eq. (24) is considered.

F. Spectral scaling properties

In the special case of a constant pulse duration, the power spectral density in Eq. (24) is fully determined by the power spectrum of the pulse function. For example, for a one-sided exponential pulse function defined in Eqs. (42) the power spectral density is given by a Lorentzian function,

$$\Omega_{\tilde{\Phi}}(\omega) = \frac{2}{1 + \omega^2}, \quad (25)$$

which has a break point at $\omega = 1$, and two asymptotic scaling regimes for the limiting frequencies: the constant value 2 in the limit $\omega \rightarrow 0$, and a $2/\omega^2$ tail in the limit $\omega \rightarrow \infty$. There is no frequency range of scale invariance characterized by exponents $0 < \beta < 2$.

Maintaining a constant pulse duration and introducing a power-law pulse function was shown to result in spectral scale invariance in a range of scaling exponents and for certain truncations of the power-law function [11]. In the following, we demonstrate that the frequency power spectral density in Eq. (24) manifests self-similar scaling for certain power-law distributions of pulse durations irrespective of the pulse function.

III. POWER-LAW DISTRIBUTED PULSE DURATIONS

In this contribution, scale invariance is introduced into the dimensionless power spectral density in Eq. (24) through the distribution of pulse durations. Several variants of power-law distributions are considered in this section. The conditions under which these distributions result in long-range dependence are then analyzed in Sec. IV. The origins of power-law distributions of pulse durations are motivated for a superposition of propagating pulses in Appendix A.

The probability densities considered here are normalized such that

$$\int_0^\infty d\tau P_\tau(\tau) = 1, \quad (26)$$

with the mean value following from Eq. (21a),

$$\langle \tau \rangle = \int_0^\infty d\tau \tau P_\tau(\tau) = 1. \quad (27)$$

A finite, nondivergent mean is required for the stationarity of the stochastic process given by Eq. (4) and for the normalization of the power spectral density in Eq. (24).

A. Variants of power-law distributions

Consider a general form of Pareto distribution with an exponent $\alpha \geq 0$,

$$P_\tau(\tau; \alpha, \tau_\downarrow, \tau_\uparrow) = \begin{cases} \eta \tau^{-\alpha} & \text{if } \tau \in [\tau_\downarrow, \tau_\uparrow], \\ 0 & \text{otherwise,} \end{cases} \quad (28)$$

where η is a normalization factor and $\tau_\downarrow < \tau_\uparrow$ are the support boundaries. Following the classification proposed in Ref. 11 for the power-law pulse function we distinguish four variants of Pareto distribution with different support truncations: unbounded $\tau \in (0, \infty)$, upper-truncated $\tau \in (0, \tau_\uparrow]$, lower-truncated $\tau \in [\tau_\downarrow, \infty)$, and bounded $\tau \in [\tau_\downarrow, \tau_\uparrow]$. The configuration of the support boundaries and the normalization conditions in Eqs. (26) and (27) determine the expressions for η , τ_\downarrow and τ_\uparrow as functions of α .

The bounded Pareto distribution will be shown most relevant for modelling long-range correlations with finite-size

effects. Its definition follows in Sec. III B, while the upper-truncated and the lower-truncated Pareto distributions are defined in Appendices B 1 and B 2, respectively. The unbounded Pareto distribution is not well defined and cannot be normalized to comply with Eq. (26). Instead, an inverse Gamma distribution is considered, as it is well defined for an unbounded support $\tau \in (0, \infty)$ due to a smooth exponential cutoff for small values of τ . The inverse Gamma distribution of pulse durations is motivated in Appendix A 4 and defined in Appendix B 3.

B. Bounded Pareto distribution

The Pareto distribution defined by Eq. (28) with a support truncated on both sides $\tau \in [\tau_\downarrow, \tau_\uparrow]$ is well defined for any $\alpha \geq 0$. Applying the condition (26) yields the following normalization factor with its limit

$$\eta(\alpha, \tau_\downarrow, \tau_\uparrow) = \frac{(\alpha - 1)(\tau_\uparrow \tau_\downarrow)^\alpha}{\tau_\uparrow^\alpha \tau_\downarrow - \tau_\uparrow \tau_\downarrow^\alpha}, \quad (29a)$$

$$\lim_{\alpha \rightarrow 1} \eta(\alpha, \tau_\downarrow, \tau_\uparrow) = \left(\ln \frac{\tau_\uparrow}{\tau_\downarrow} \right)^{-1}. \quad (29b)$$

The bounded Pareto distribution has a total of three parameters $\{\alpha, \tau_\downarrow, \tau_\uparrow\}$ subject to the conditions (26) and (27). We thus reduce the number of parameters by introducing the ratio of the two support boundaries as a new dimensionless parameter,

$$\Delta = \frac{\tau_\uparrow}{\tau_\downarrow}, \quad (30)$$

where it follows that $\Delta > 1$. The parameter Δ describes the logarithmic width of the bounded Pareto distribution, where $\log_{10} \Delta$ gives the number of logarithmic decades spanned by the support.

The normalization factor and its limit given by Eqs. (29) are expressed in terms of α and Δ as

$$\eta(\alpha, \Delta) = \frac{(\alpha - 1)}{1 - \Delta^{1-\alpha}} \tau_\downarrow^{\alpha-1}, \quad (31a)$$

$$\lim_{\alpha \rightarrow 1} \eta(\alpha, \Delta) = \frac{1}{\ln \Delta}. \quad (31b)$$

The resulting mean of the bounded Pareto distribution normalized according to the condition (27) yields the two support boundaries with their respective limits,

$$\tau_\downarrow(\alpha, \Delta) = \frac{(\alpha - 2)(1 - \Delta^{1-\alpha})}{(\alpha - 1)(1 - \Delta^{2-\alpha})}, \quad (32a)$$

$$\lim_{\alpha \rightarrow 1} \tau_\downarrow(\alpha, \Delta) = \frac{\ln \Delta}{\Delta - 1}, \quad (32b)$$

$$\lim_{\alpha \rightarrow 2} \tau_\downarrow(\alpha, \Delta) = \frac{\Delta - 1}{\Delta \ln \Delta}, \quad (32c)$$

$$\tau_\uparrow(\alpha, \Delta) = \Delta \tau_\downarrow(\alpha, \Delta). \quad (32d)$$

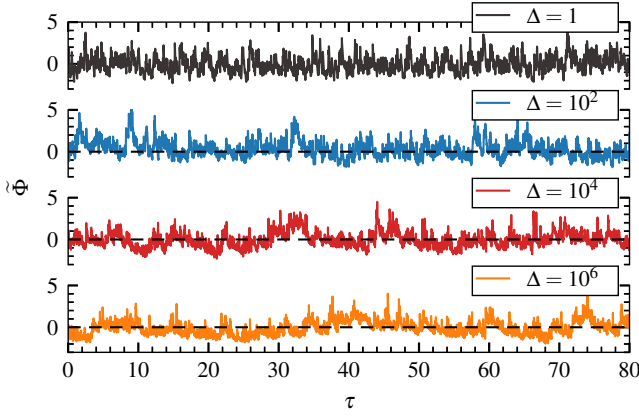


FIG. 1. Normalized realizations of the stochastic process for a one-sided exponential pulse function, pulse overlap parameter $\gamma = 10$, and a bounded Pareto distribution of pulse durations with exponent $\alpha = 2$. Consecutive realizations are obtained for different distribution widths Δ .

The bounded Pareto distribution is thus parametrized as $P_\tau(\tau; \alpha, \Delta)$. This definition is aligned with Eq. (A14) motivated in Appendix A 3 for the dimensional variable. The variance of the pulse duration is then given by

$$\langle \tau^2 \rangle(\alpha, \Delta) = \frac{(\alpha - 2)(1 - \Delta^{3-\alpha})}{(\alpha - 3)(1 - \Delta^{2-\alpha})} \tau_\downarrow, \quad (33)$$

with the following finite limits

$$\lim_{\alpha \rightarrow 1} \langle \tau^2 \rangle(\alpha, \Delta) = \frac{(\Delta + 1) \ln \Delta}{2(\Delta - 1)}, \quad (34a)$$

$$\lim_{\alpha \rightarrow 2} \langle \tau^2 \rangle(\alpha, \Delta) = \frac{(\Delta - 1)^2}{\Delta \ln^2 \Delta}, \quad (34b)$$

$$\lim_{\alpha \rightarrow 3} \langle \tau^2 \rangle(\alpha, \Delta) = \frac{(\Delta + 1) \ln \Delta}{2(\Delta - 1)}. \quad (34c)$$

The variance and the parameters of the distribution determine the long-range dependence characteristics of the associated process, as will be discussed in Sec. IV.

Figure 1 shows realizations of the process defined by Eq. (4) for the bounded Pareto distribution of pulse durations for $\alpha = 2$ and different values of Δ . The top curve for $\Delta = 1$ corresponds to a process with a constant pulse duration, characterized by a Lorentzian power spectral density given by Eq. (25). Extending the width of the distribution entails an increase in the upper bound in Eq. (32d). The resulting introduction of pulses with relatively long durations is manifested as low-frequency fluctuations, which in Fig. 1 become gradually more pronounced as the value of Δ is increased. Importantly, the extent to which broadening of the distribution width affects the upper bound of the distribution and the long-range dependence characteristics of the process depends on the value of α . This is demonstrated in Fig. 2 and further addressed in Sec. IV B.

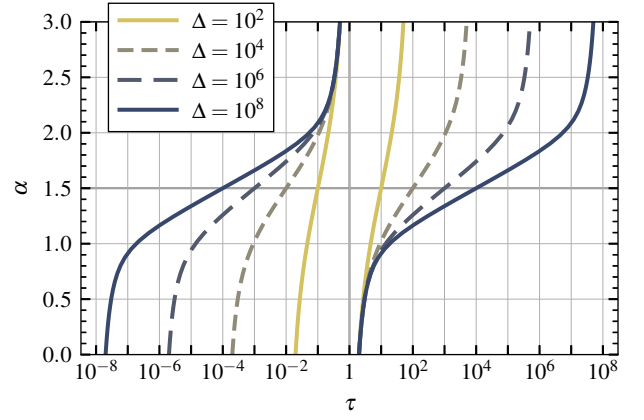


FIG. 2. Range of normalized pulse durations τ for a bounded Pareto distribution and various width parameters Δ . Each pair of corresponding curves marks the boundaries τ_\downarrow and τ_\uparrow for a given distribution width Δ and with the power-law exponent α varying in the range $\alpha \in [0, 3]$. Pulse durations are normalized with the mean value.

IV. CONDITIONS FOR LONG-RANGE DEPENDENCE

The scale invariance of the frequency power spectral density is related to the self-similarity properties of the underlying distribution of pulse durations. In this section, we consider the distributions defined in Sec. III and Appendix B, and we identify the parameter ranges at which long-range dependence is expected to emerge. The results are summarized in Table I.

A. Infinite variance

Long-range correlations are typically well represented by processes with infinite variance. For the lower-truncated Pareto and the inverse Gamma distributions the dimensional pulse duration s is characterized by a finite mean value and an infinite variance for $2 < \alpha \leq 3$. For $\alpha \leq 2$ the mean value is infinite, preventing the normalization of the power spectral density Ω_Φ given by Eq. (24). These findings are reflected in the last two columns of Table I.

For the upper-truncated Pareto and the bounded Pareto distributions the variance of the pulse durations is finite for all values of α . However, this does not preclude long-range dependence resulting from these finite-support distributions. In the following we discuss further distribution aspects that may promote spectral scale invariance and long-range correlations.

B. Long pulse durations

Pulses with long durations obviously contribute to long-range dependence. Allowing arbitrarily long pulse durations requires a divergence of the upper bound, $\tau_\uparrow \rightarrow \infty$. For the upper-truncated Pareto distribution, the upper bound given by Eq. (B2) diverges towards infinity only in the limit $\alpha \rightarrow 1^-$. In this limit the distribution itself is not well defined. The power spectral density of a process with an upper-truncated Pareto

distribution of pulse durations is thus not expected to manifest scale invariance. This is indicated in the first column of Table I.

In the case of the bounded Pareto distribution, both support boundaries are modified simultaneously and indirectly, through the parameter Δ given by Eq. (30). Changing the value of Δ affects the behavior of τ_{\downarrow} and τ_{\uparrow} differently depending on the value of α . In particular, in the limit $\Delta \rightarrow \infty$ the lower and the upper bounds given by Eqs. (32), as well as the normalization factor given by Eq. (31), have the following limits

$$\lim_{\Delta \rightarrow \infty} \tau_{\downarrow}(\alpha, \Delta) = \begin{cases} 0 & \text{if } \alpha \leq 2, \\ \frac{\alpha-2}{\alpha-1} & \text{if } \alpha > 2, \end{cases} \quad (35a)$$

$$\lim_{\Delta \rightarrow \infty} \tau_{\uparrow}(\alpha, \Delta) = \begin{cases} \frac{\alpha-2}{\alpha-1} & \text{if } \alpha < 1, \\ \infty & \text{if } \alpha \geq 1, \end{cases} \quad (35b)$$

$$\lim_{\Delta \rightarrow \infty} \eta(\alpha, \Delta) = \begin{cases} -\frac{(\alpha-2)^{\alpha-1}}{(\alpha-1)^{\alpha-2}} & \text{if } \alpha < 1, \\ 0 & \text{if } 1 \leq \alpha \leq 2, \\ \frac{(\alpha-2)^{\alpha-1}}{(\alpha-1)^{\alpha-2}} & \text{if } \alpha > 2. \end{cases} \quad (35c)$$

Equations (35) indicate that in the limit $\Delta \rightarrow \infty$ the bounded Pareto distribution approaches the upper-truncated Pareto distribution when $\alpha < 1$, and approaches the lower-truncated Pareto distribution when $\alpha > 2$. In the range $1 \leq \alpha \leq 2$ the lower and the upper bounds approach zero and infinity respectively, while the normalization factor vanishes, ensuring that the normalization condition (27) is met.

The placement of the support bounds with respect to the mean value is demonstrated in Fig. 2 for various values of the width parameter Δ and for scaling exponents $\alpha \in [0, 3]$. For $\alpha < 1$ the increase in Δ implies the decrease of the lower bound τ_{\downarrow} with respect to the mean value, while the upper bound τ_{\uparrow} remains at the order of magnitude of the mean value. The opposite is true for $\alpha > 2$, where τ_{\uparrow} increases with respect to the mean value while τ_{\downarrow} remains close to the mean value. Figure 2 shows a smooth transition between these two regimes. At $\alpha = 3/2$ both τ_{\downarrow} and τ_{\uparrow} are at equal logarithmic distance from the mean value.

Considering the divergence of the upper bound as the driver of long-range dependence, Eq. (35b) suggests that $\alpha \geq 1$ is necessary for arbitrarily long pulse durations to emerge from a sufficiently wide bounded Pareto distribution. As the value of Δ approaches infinity, the pulse duration variance given by Eq. (34) has the following limits

$$\lim_{\Delta \rightarrow \infty} \langle \tau^2 \rangle(\alpha, \Delta) = \begin{cases} \infty & \text{if } 1 \leq \alpha \leq 3, \\ \frac{(\alpha-2)^2}{(\alpha-3)(\alpha-1)} & \text{otherwise.} \end{cases} \quad (36)$$

Long-range dependence is thus expected in the exponent range $1 \leq \alpha \leq 3$.

As the power-law exponent increases beyond $\alpha = 3$, the bounded Pareto distribution narrows and assumes the shape of a degenerate distribution corresponding to constant pulse duration. Conversely, in the limit $\alpha \rightarrow 0$ the bounded Pareto distribution reduces to a uniform distribution, with no long-range correlations involved [27].

TABLE I. Existence of the probability density function and the two lowest-order moments for pulse durations at different values of exponent α . Colored shading indicates the anticipated self-similar scaling of the power spectral density due to infinite variance.

	P_{τ} Pareto			P_{τ} inverse Gamma
	$\tau \in (0, \tau_{\uparrow}]$	$\tau \in [\tau_{\downarrow}, \tau_{\uparrow}]$	$\tau \in [\tau_{\downarrow}, \infty)$	$\tau \in (0, \infty)$
$0 < \alpha < 1$	$\langle \tau^2 \rangle < \infty$	$\lim_{\Delta \rightarrow \infty} \langle \tau^2 \rangle < \infty$	no P_s	
$\alpha = 1$	no P_s	$\lim_{\Delta \rightarrow \infty} \tau_{\uparrow} = \infty$		
$1 < \alpha \leq 2$			$\lim_{\Delta \rightarrow \infty} \tau_{\uparrow} = \infty$	$\langle s \rangle = \infty$
$2 < \alpha < 3$		$\lim_{\Delta \rightarrow \infty} \langle \tau^2 \rangle = \infty$	$\langle \tau^2 \rangle = \infty$	
$\alpha = 3$		$\lim_{\Delta \rightarrow \infty} \langle \tau^2 \rangle < \infty$	$\langle \tau^2 \rangle < \infty$	
$\alpha > 3$				

Long-range dependence is anticipated for the distributions which allow for arbitrarily long pulse durations, and in the range of exponents α where the pulse duration variance is infinite. The bounded Pareto distribution represented in the second column of Table I satisfies both conditions for the widest range of exponents α . These predictions are verified in Sec. V, where the corresponding Table II summarizes the signatures of scale invariance demonstrated for the analytical power spectral density expressions.

C. Scaling exponents relation

In the following, we explore the relation between the exponent α of the general Pareto distribution in Eq. (28) and the scaling exponent of the power spectral density given by Eq. (24). The general Pareto distribution displays scale invariance in the unbounded limit

$$\lim_{\substack{\tau_{\downarrow} \rightarrow 0 \\ \tau_{\uparrow} \rightarrow \infty}} P_{\tau}(\kappa\tau) = \lim_{\substack{\tau_{\downarrow} \rightarrow 0 \\ \tau_{\uparrow} \rightarrow \infty}} \kappa^{-\alpha} P_{\tau}(\tau), \quad (37)$$

where κ is a scaling factor. Similarly, rescaling the frequency of the power spectral density by a factor κ gives

$$\Omega_{\tilde{\Phi}}(\kappa\omega) = \int_0^{\infty} d\tau \tau^2 P_{\tau}(\tau) \varrho_{\Phi}(\kappa\tau\omega). \quad (38)$$

Inserting the general form of the Pareto distribution into Eq. (38), making a change of variable $\tau' = \kappa\tau$, and applying the scaling relation in Eq. (37) gives

$$\Omega_{\tilde{\Phi}}(\kappa\omega) = \kappa^{\alpha-3} \int_0^{\infty} d\tau' \tau'^2 P_{\tau}(\tau') \varrho_{\Phi}(\tau'\omega). \quad (39)$$

It follows from Eqs. (38) and (39) that in the limit of an infinitely broad distribution of pulse durations, where Eq. (37) applies, the frequency power spectral density displays scale invariance [31],

$$\lim_{\substack{\tau_{\downarrow} \rightarrow 0 \\ \tau_{\uparrow} \rightarrow \infty}} \Omega_{\tilde{\Phi}}(\kappa\omega) = \lim_{\substack{\tau_{\downarrow} \rightarrow 0 \\ \tau_{\uparrow} \rightarrow \infty}} \kappa^{\alpha-3} \Omega_{\tilde{\Phi}}(\omega). \quad (40)$$

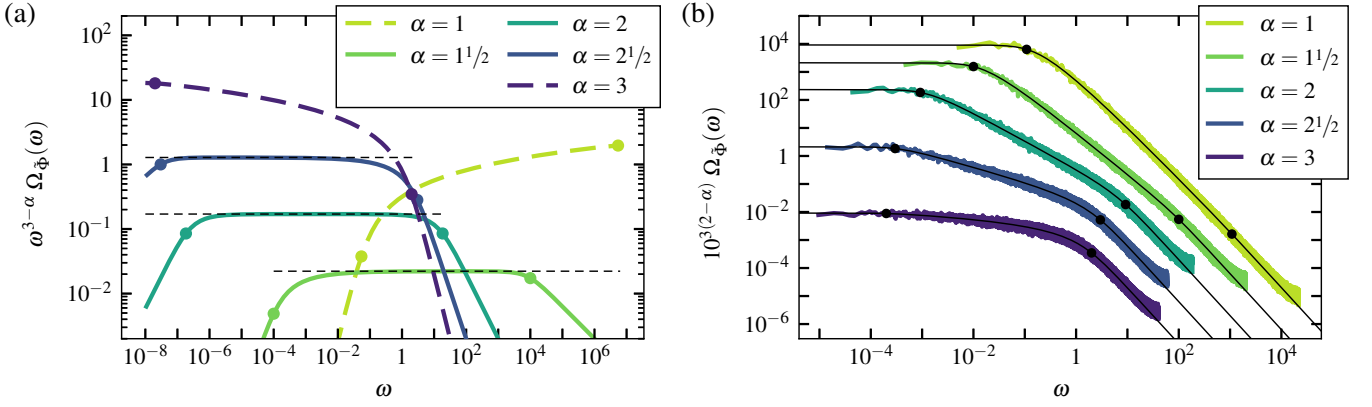


FIG. 3. Power spectral densities for a super-position of one-sided exponential pulses with bounded-Pareto distributed durations. Filled circles mark the cutoff frequencies $\omega\tau_{\uparrow} = 1$ and $\omega\tau_{\downarrow} = 1$. The presented values of α span the entire exponent range associated with spectral scale invariance obtained for the bounded Pareto distribution. (a) Compensated analytical power spectral densities $\omega^{3-\alpha} \Omega_{\Phi}(\omega; \alpha)$ with Ω_{Φ} given by Eq. (46) for $\Delta = 10^8$. The horizontal dashed black lines mark the inverse of the ω -independent factors in Eqs. (47b)–(47d). The regions where the dashed black lines overlap with the solid colored lines indicate constant compensated spectra, and hence denote the frequency ranges where frequency scaling $1/\omega^{3-\alpha}$ is manifested. The compensated spectra plotted with thick dashed colored lines are the ones where the logarithmic corrections to the frequency scaling apply, according to Eqs. (47a) and (47e). (b) Empirical power spectral densities for realizations of the process with $\Delta = 10^4$. The respective analytical power spectral densities are plotted with solid black curves. Vertical shifting by α -dependent factors is applied to avoid overlapping.

Equation (40) suggests that the power spectral density itself has a power-law signature $\Omega_{\Phi}(\omega) \sim 1/\omega^{\beta}$ with

$$\beta(\alpha) = 3 - \alpha. \quad (41)$$

If $\Omega_{\Phi}(\omega)$ displays scale invariance, then it follows from Sec. IV B that long-range correlations are expected in the limit $\Delta \rightarrow \infty$ and within the range of Pareto exponents $1 \leq \alpha \leq 3$. According to Eq. (41), this corresponds to the range of frequency scaling exponents $0 \leq \beta \leq 2$, where $\beta = 0$, $\beta = 1$ and $\beta = 2$ are exponents characteristic of white, pink, and Brownian noises, respectively. The frequency range in which bounded spectral scale invariance is anticipated is determined by the range of the underlying pulse durations, with the delimiting angular frequencies given by $1/\tau_{\uparrow}$ and $1/\tau_{\downarrow}$. Outside this range the shape of the power spectral density is determined by the power spectral density of the pulse function, $\varrho_{\Phi}(\tau\omega)$, resulting in a broken power law with break points at the cutoff frequencies.

V. SCALE INVARIANCE OF POWER SPECTRA

In the following, we apply the pulse duration distributions described in Sec. III to the general expression for the frequency power spectral density in Eq. (24). We derive explicit, closed-form expression for the power spectral density $\Omega_{\Phi}(\omega; \alpha, \Delta)$ parametrized by the scaling exponent α and the distribution width Δ . We expose analytically the universal $1/\omega^{3-\alpha}$ signature emerging for the parameter regimes discussed in Sec. IV, and we demonstrate the finite-size effects associated with the truncations of the underlying distributions.

A. Pulse function

The power spectral density formulas presented in this section are derived for a one-sided exponential pulse function ϕ defined below together with its auto-correlation function ρ_{ϕ} , and the respective Lorentzian power spectral density ϱ_{ϕ} [27],

$$\phi(\theta) = \Theta(\theta) \exp(-\theta), \quad (42a)$$

$$\rho_{\phi}(\theta) = \exp(-|\theta|), \quad (42b)$$

$$\varrho_{\phi}(\vartheta) = \frac{2}{1 + \vartheta^2}, \quad (42c)$$

where Θ is the unit step function

$$\Theta(\theta) = \begin{cases} 1 & \text{if } \theta \geq 0, \\ 0 & \text{if } \theta < 0. \end{cases} \quad (43)$$

The pulse function and its power spectral density are respectively normalized as

$$\int_{-\infty}^{\infty} d\theta |\phi(\theta)| = 1, \quad (44a)$$

$$\int_{-\infty}^{\infty} d\vartheta \varrho_{\phi}(\vartheta) = 2\pi, \quad (44b)$$

resulting in the following normalization of the power spectral density given by Eq. (24),

$$\int_{-\infty}^{\infty} d\omega \Omega_{\Phi}(\omega) = 2\pi. \quad (45)$$

These normalization constraints are satisfied for all the power spectral densities considered in the following. The presence of spectral scale invariance for other pulse functions is discussed in Sec. VIB 5.

B. Power spectral density for the bounded Pareto distribution of pulse durations

Applying the bounded Pareto distribution given by Eqs. (28) and (31)–(32) to the power spectral density given by Eq. (24) we obtain [31]

$$\Omega_{\tilde{\Phi}}(\omega; \alpha, \Delta) = \begin{cases} \frac{1}{\ln \Delta \omega^2} \ln \left(\frac{(\Delta-1)^2 + (\Delta \ln \Delta \omega)^2}{(\Delta-1)^2 + (\ln \Delta \omega)^2} \right) & \text{if } \alpha = 1, \\ \frac{2}{\ln \Delta \omega} \left[\arctan \left(\frac{(\Delta-1)\omega}{\ln \Delta} \right) - \arctan \left(\frac{(\Delta-1)\omega}{\Delta \ln \Delta} \right) \right] & \text{if } \alpha = 2, \\ \frac{2}{(\Delta^\alpha - \Delta)\omega^2} \left[\Delta^\alpha {}_2F_1 \left(1, \frac{\alpha-1}{2}, \frac{\alpha+1}{2}; -\frac{1}{\tau_\uparrow^2 \omega^2} \right) - \Delta {}_2F_1 \left(1, \frac{\alpha-1}{2}, \frac{\alpha+1}{2}; -\frac{1}{\tau_\downarrow^2 \omega^2} \right) \right] & \text{otherwise,} \end{cases} \quad (46)$$

where τ_\downarrow and τ_\uparrow are given by Eqs. (32). An explicit power spectral density expression equivalent to Eq. (46) was presented in Ref. 18 for a Poisson process with distributed pulse decay rates.

Considering the compensated spectra in the limit of an infinitely broad distribution of pulse durations for various exponents reveals power law scalings [31],

$$\lim_{\Delta \rightarrow \infty} \Omega_{\tilde{\Phi}}(\omega; 1, \Delta) \omega^2 \frac{\ln \Delta}{\ln(\omega^2 \ln^2 \Delta)} = 1, \quad (47a)$$

$$\lim_{\Delta \rightarrow \infty} \Omega_{\tilde{\Phi}}(\omega; 3/2, \Delta) |\omega|^{3/2} \frac{\sqrt{2}(\sqrt{\Delta}-1)}{\pi \sqrt[4]{\Delta}} = 1, \quad (47b)$$

$$\lim_{\Delta \rightarrow \infty} \Omega_{\tilde{\Phi}}(\omega; 2, \Delta) |\omega| \frac{\ln \Delta}{\pi} = 1, \quad (47c)$$

$$\lim_{\Delta \rightarrow \infty} \Omega_{\tilde{\Phi}}(\omega; 5/2, \Delta) |\omega|^{1/2} \frac{\sqrt{6}(\sqrt{\Delta}-1)}{\pi \sqrt{1+\sqrt{\Delta}+\Delta}} = 1, \quad (47d)$$

$$\lim_{\Delta \rightarrow \infty} \Omega_{\tilde{\Phi}}(\omega; 3, \Delta) 2 \left[\ln \left(1 + \frac{4}{\omega^2} \right) \right]^{-1} = 1. \quad (47e)$$

In particular, Eq. (47c) reveals the $1/\omega$ signature of the pink noise obtained for $\alpha = 2$ [18, 31]. The above equation confirms the anticipated scale invariance $1/\omega^{3-\alpha}$ of the frequency power spectral density for $1 < \alpha < 3$. At the boundaries of the scale-invariance regime, $\alpha = 1$ and $\alpha = 3$, logarithmic corrections to the frequency scaling occur. Similar logarithmic corrections in a closed-form power spectral density have been shown for a renewal process with power-law-distributed waiting times [14].

Figure 3(a) shows the compensated spectra corresponding to Eqs. (47) for a distribution width $\Delta = 10^8$. The filled circles mark the cutoff frequencies $\omega\tau_\uparrow = 1$ and $\omega\tau_\downarrow = 1$ delimiting the theoretical frequency range of self-similar scaling for each value of α . No signatures of scale invariance are exposed for the cases $\alpha = 1$ and $\alpha = 3$, where logarithmic corrections to the frequency scaling apply. The $1/\omega^{3-\alpha}$ scaling is clearly manifested for the remaining Pareto exponents, $\alpha \in \{1^{1/2}, 2, 2^{1/2}\}$. The thin dashed lines in Fig. 3(a) mark the inverse of the ω -independent factors in Eqs. (47b)–(47d) indicating the constant levels which the compensated

TABLE II. Scaling signatures of the power spectral density $\Omega_{\tilde{\Phi}}$ for different exponents α of power-law distributions of pulse durations P_τ .

	P_τ Pareto			P_τ inverse Gamma
	$\tau \in (0, \tau_\uparrow]$	$\tau \in [\tau_\downarrow, \tau_\uparrow]$	$\tau \in [\tau_\downarrow, \infty)$	$\tau \in (0, \infty)$
$0 < \alpha < 1$	$\sim 1/\omega^{3-\alpha}$			no P_s
$\alpha = 1$	no P_s	log corr.	$\langle s \rangle = \infty$	
$1 < \alpha \leq 2$				
$2 < \alpha < 3$		$\sim 1/\omega^{3-\alpha}$		
$\alpha = 3$		log corr.		
$\alpha > 3$		$\sim 1/\omega^{3-\alpha}$		

power spectral densities approach asymptotically in the limit of an infinitely broad region of scale invariance. Notably, the exposed $1/\omega^{3-\alpha}$ scaling vanishes towards the cutoff frequencies. Figure 3(a) demonstrates that in the case of a finite-size scale invariance, the effective frequency range of self-similar scaling is reduced by approximately two to three logarithmic decades with respect to the Δ -range of the underlying distribution of pulse durations [31]. This reduction is attributed to the gradual transitions between the distinct regions of a broken power law.

Figure 3(b) presents the empirical power spectral densities obtained from realizations of the process for bounded Pareto distributions with narrower support characterized by $\Delta = 10^4$. The normalized sampling and duration intervals are relative to the support boundaries and equal to $\tau_\downarrow/40$ and $640\tau_\uparrow$, respectively. The broken power-law transitions at $\omega\tau_\downarrow = 1$ and $\omega\tau_\uparrow = 1$ are then resolved with a one-decade margin using the Welch's method. Each process realization comprises of more than 80000 pulses, with the total number of pulses being proportional to the interval of duration and the pulse overlap parameter, here $\gamma = 10$. We recall that the analytical power spectral density expression in Eq. (24) is independent of parameter γ . The empirical results in Fig. 3(b) agree with the corresponding analytical predictions, including the cases where logarithmic corrections to the frequency scaling apply.

Analogous analyses of the scale invariance of the frequency power spectral densities obtained for the upper-truncated Pareto, the lower-truncated Pareto, and the inverse Gamma distributions of pulse durations are presented in Appendix B. The parameter regimes for which the $1/\omega^{3-\alpha}$ scaling is manifested are summarized in Table II for all the considered distribution variants. The results are discussed in Sec. VI B.

VI. DISCUSSION

The findings presented in this contribution are first related to the previous works addressing scale invariance of the frequency power spectral density for a superposition of uncorrelated pulses with distributed durations. The regimes of va-

validity of the $1/\omega^{3-\alpha}$ scaling are then discussed based on the results presented in Secs. IV and V.

A. Relation to previous works

We revisit the previous pivotal works regarding spectral scaling due to distributed pulse durations and decay rates. We highlight the elements that these works fail to address, and which we in this contribution show to be of relevance for describing the emergence of spectral scale invariance.

1. Power spectra for distributed pulse durations and decay rates

Distributed pulse decay rates $v = 1/\tau$ can be equivalently considered for a process defined by Eq. (4). The associated power spectral density is obtained analogously by statistical averaging, or directly from Eq. (24) using the probability of the inverse variable $P_v(v)$ according to Eq. (A6),

$$\Omega_{\Phi}(\omega) = \int_0^{\infty} dv v^{-2} P_v(v) \varrho_{\Phi}(\omega/v). \quad (48)$$

For $P_{\tau}(\tau) \sim \tau^{-\alpha}$ it follows that $P_v(v) \sim v^{-(2-\alpha)}$. Denoting $\lambda = 2 - \alpha$, the scaling relation in Eq. (41) becomes

$$\beta = 3 - \alpha = 1 + \lambda. \quad (49)$$

The distribution of pulse decay rates $P_v(v)$ defined on a bounded support $v \in [v_{\downarrow}, v_{\uparrow}]$ is for $\lambda = 0$ reduced to a uniform distribution, which results in $1/\omega$ scaling of the power spectral density [18]. Obtaining a $1/\omega^{\beta}$ signature with $\beta \neq 1$ requires explicit power-law scalings in the distributions of pulse durations or decay rates. Relating P_v and P_{τ} is not generally trivial due to few known distribution pairs with explicit expressions for the forward and inverse transformations.

2. Approach of van der Ziel

As outlined in Sec. I, the approach for deriving the power spectral density of a process with distributed pulse durations from the auto-correlation function of a process where all pulses have the same duration does not account for internal long-range correlations resulting from the overlap of long-lasting, uncorrelated pulses. Such an approach, attributed to van der Ziel [19], implies that the spectral scaling is proportional to $1/\omega^{2-\alpha}$ and thus that $P_{\tau}(\tau) \sim 1/\tau$ underlies $1/f$ noise. This result was challenged by Butz [20], and it is also incongruous with the analysis presented in this contribution demonstrating $1/\omega^{3-\alpha}$ spectral scaling of the frequency power spectral density.

Acknowledging the experimental results presented in Ref. 22, speaking to the theory of van der Ziel, requires distinguishing between a superposition of interacting pulses with continuously distributed durations, and an aggregation of processes with respective constant durations. Hooze and Bobbert argue that summation of spectra is valid only for isolated processes [32, 33]. They consider an example of a

generation-recombination process in an n -type semiconductor with a range of traps whose characteristic times τ are distributed as $P_{\tau}(\tau) \sim 1/\tau$ in a wide range. The spectrum of the process is then shown to scale as $1/\omega$ only if the individual traps are isolated, while in the presence of interactions (transitions) between the traps the spectrum has Lorentzian characteristics, which agrees with the results presented here. The authors then remark that the isolation condition is seldom considered when interpreting $1/f$ noises in electronic devices.

Unquestionably, van der Ziel and his contemporaries contributed with a large body of theoretical and experimental work to the field of flicker noise modelling [19, 34–40]. However, due to the inherent differences in the dynamics of isolated and interacting processes this theory has a limited scope of applicability. Recognizing this is essential for selecting a representative theoretical framework.

3. Work of Butz

Butz derives a power spectral density integral for a process with a general pulse function and an arbitrary distribution of pulse decay rates, corresponding to Eq. (48) [20]. He relates pulse decay rates and durations, and demonstrates that the $1/\omega$ spectrum arises from uniformly-distributed decay rates, or equivalently from durations distributed as $1/\tau^2$. With this he highlights the distinction with respect to the work of van der Ziel. Butz then argues for a strict $1/\omega$ spectrum in the limit of small frequencies, or long pulse durations. Only asymptotic scaling relations are discussed in Ref. 20 and no closed-form power spectral density expressions are offered. Therefore, there is neither any consideration of the finite-size effects discussed in this contribution. For a power-law distribution of pulse decay rates, Butz derives a scaling relation equivalent to Eq. (49) without considering the range of exponents for which it is valid.

4. Work of Milotti

Milotti considers a Poisson process as a framework for developing an exact numerical method for simulating colored noises [18]. He derives a closed-form power spectral density for a superposition of pulses with a one-sided exponential shape and a bounded Pareto distribution of decay rates. He presents the explicit expression for the case of a uniform distribution of decay rates, demonstrating the $1/\omega$ scaling. An analogous closed-form expression was presented by van der Ziel in Ref. 36 for $P_{\tau}(\tau) \sim 1/\tau$, which corresponds to $P_v(v) \sim 1/v$ distribution of decay rates, reflecting the aforementioned discrepancies in the predicted scalings. The closed-form power spectral densities presented by Milotti correspond respectively to the third and the second case of Eq. (46).

Milotti furthermore states that a scaling relation equivalent to Eq. (49) is applicable in a range of frequencies delimited by the minimum and maximum decay rates. Finite-size effects associated with the cutoff frequencies are not considered.

There is no discussion of the divergence of the lower and the upper bounds of the Pareto distribution, or the existence of the distribution and the mean duration in the relevant limits. No connection between the infinite variance of the pulse decay rate and the spectral scale invariance is made. The exponent range in which the $\beta = 1 + \lambda$ scaling is valid is not considered, and no logarithmic corrections to the frequency scalings are exposed.

Milotti presents empirical power spectral densities with $1/\omega$ and $1/\omega^{1.2}$ signatures obtained for Pareto distributions spanning four logarithmic decades. The broken power-law transitions at the minimum and maximum decay rates are not fully resolved. The minimum distribution width necessary for a region of self-similar frequency scaling to emerge is not considered. We recognize that the main focus of Ref. 18 is describing the details of the numerical generator of power-law noises. The analytical results with finite-size effects presented here therefore complement and extend the works of van der Ziel, Butz and Milotti.

B. Regimes of validity of the $1/\omega^{3-\alpha}$ scaling

The previous works considering spectral scaling for a super-position of uncorrelated pulses with distributed durations or decay rates have not addressed the conditions necessary for long-range dependence to emerge. The regimes of validity of the $1/\omega^{3-\alpha}$ scaling are examined here.

1. Characteristics of pulse duration distribution

Table II summarizes the scaling properties of the power spectral densities obtained for different distributions of pulse durations for different ranges of the exponent α . Consistent with the expectations from Table I, the $1/\omega^{3-\alpha}$ scaling is manifested only if the variance of the pulse duration is infinite, which implies that the distribution allows for arbitrarily long pulse durations. This includes the bounded Pareto distribution in the limit of infinitely broad support. Figure 3(a) exposes an effective $1/\omega^{3-\alpha}$ scaling also for the bounded Pareto distribution with finite but wide support. A bounded Pareto distribution with a narrow support does not result in spectral scale invariance due to finite-size effects discussed in Secs. VIB 3 and VIB 4.

A similar classification of spectral scaling characteristics was presented in Ref. 11 for a filtered Poisson process with a bounded power-law pulse function. Denoting the power-law exponent as α , the resulting scale invariance was shown to follow the relation $\beta = 2(1 - \alpha)$ for $0 < \alpha < 1$ given a non-divergent upper cutoff of the power-law pulse function. A different study addressing spectral scale invariance in fractal renewal processes with power-law distributed inter-event times demonstrated that processes with alternating values follow the $\beta = 3 - \alpha$ relation for $1 < \alpha < 3$, with logarithmic corrections to the frequency scaling at $\alpha = 3$ [14]. This range of power-law exponents is the same as the one obtained in this contribution for the power-law distributed pulse durations. It was

further shown in Ref. 14 that fractal renewal processes with Dirac delta pulses follow the $\beta = 3 - \alpha$ relation for $2 < \alpha < 3$, and the $\beta = \alpha - 1$ relation for $1 < \alpha < 2$, with logarithmic corrections to the frequency scaling at the upper bounds of the respective ranges, $\alpha = 3$ and $\alpha = 2$. Both of the latter scaling regimes result in a range of spectral scaling exponents $\beta \in (0, 1)$.

2. Low-frequency cutoff

The divergence of the upper bound $\tau_{\uparrow} \rightarrow \infty$ entails that the region of spectral scale invariance has no cutoff at low frequencies. The integrability of the associated power spectral density then requires $\alpha > 2$, equivalent to $\beta > 1$. This leads to a paradox where Parseval's identity is seemingly violated by empirical $1/f$ noises observed in physical systems where no upper bound on the scale of events can be identified, except for the observation time itself. The paradox has been resolved for intermittency-induced scale invariance with aging power spectra [17, 41–43].

Unlike inter-event times, event durations are limited by finite energies fueling physical process, hence the low-frequency cutoff is always expected to occur. Furthermore, the paradox does not apply as soon as $\alpha > 2$, for example at $\alpha = 2^{1/100}$ featured in Figs. 6(a) and 6(c). The resulting spectral scaling would hardly be distinguishable from an exact $1/f$ noise in empirical power spectral densities obtained for physical measurement signals.

3. Logarithmic corrections to the frequency scaling

Logarithmic corrections to the frequency scaling at $\alpha = 1$ and $\alpha = 3$ are exposed for all power spectral densities in Sec. V. Spectral scale invariance is thus not manifested at the boundaries of the long-range dependence regime, $\beta = 0$ and $\beta = 2$. The frequency range of self-similar scaling shortens gradually as the power-law exponent approaches $\alpha \rightarrow 1^+$ or $\alpha \rightarrow 3^-$. This is seen in Figs. 6(a) and 6(c) where the onset of power-law scaling shifts towards lower frequencies for increasing values of α . Scale invariance occurring in frequency ranges bounded on both sides vanishes completely for $|\alpha - 2| \gtrsim 6/7$, where the scaling relation in Eq. (49) effectively no longer holds [31]. Self-similar scaling with logarithmic corrections is then regarded as the final stage of transitioning to regular dynamics characterized by exponents $\beta \notin (0, 2)$. The presence of logarithmic corrections are well known for phase transitions and critical behavior [44–46]. Recently, it has also been demonstrated for the case of nonoverlapping, rectangular structures with power law distributed durations [21].

4. Bounded scale invariance

Size limitations applying to physical systems and measurements result in truncations of the pulse duration distributions,

which then manifest as broken power-law transitions in the frequency power spectral density. Spectral characteristics outside the frequency range of scale invariance are dictated by the pulse function. For a one-sided exponential pulse function, Lorentzian characteristics are displayed at the limiting frequencies [27].

Figure 3(a) demonstrates the extent to which the frequency ranges of an effective $1/\omega^{3-\alpha}$ scaling are reduced due to the curvature associated with the broken power-law transitions. The curvature is comparable for both the abrupt and the gradual cutoffs of the underlying distributions, as shown respectively in Figs. 6(a) and 6(c), which are discussed in Appendix B. Self-similar scaling does not manifest unless at least four decades of underlying power-law scaling are present [31]. Logarithmic-correction effects discussed in Sec. VIB 3 contribute to a further reduction of the scale invariance regions, to an extent depending on the value of α . The presence of persistent power-law scaling is confirmed by compensated spectra.

5. Pulse function characteristics

If the exponent of pulse duration distribution does not result in a $1/\omega^{3-\alpha}$ signature, the spectral characteristics are fully determined by the pulse function. The power spectral densities obtained for a one-sided exponential pulse function presented in Sec. V demonstrate Lorentzian characteristics for $\alpha \notin [1, 3]$. In particular, asymptotic constant scaling in the low-frequency limit, and an asymptotic $1/\omega^2$ scaling in the high-frequency limit has been analytically confirmed for: the upper-truncated Pareto distribution with $\alpha = 0$; the lower-truncated Pareto and the inverse Gamma distributions with $\alpha = 4$; the bounded Pareto distribution with $\alpha = 0$ and $\alpha = 4$ in the limits $\Delta \rightarrow 1$ and $\Delta \rightarrow \infty$.

In general, the upper bound for the range of exponents β satisfying the $\beta = 3 - \alpha$ relation is determined by the pulse function and the distribution of pulse durations. The steepness of the spectral scaling at high frequencies is determined by the highest-energy component. A one-sided exponential pulse function contributes with $1/\omega^2$ spectral tail, preventing the manifestation of scaling signatures characterized by $\beta > 2$. The lower-truncated Pareto and the inverse Gamma distributions require $\alpha > 2$ for a finite mean value, which further reduces the range of observable exponents to $0 \leq \beta < 1$. We recall that the lower bound $\beta = 0$ is imposed by the condition of infinite variance of the pulse duration, $\alpha \leq 3$.

Alternative pulse functions characterized by steeper spectral tails allow for manifestation of $1/\omega^{3-\alpha}$ scaling also for $\beta > 2$, if combined with pulse duration distributions whose mean value is finite for $\alpha < 1$, such as the bounded Pareto distribution or the upper-truncated Pareto distribution. Examples of relevant pulse functions include: a two-sided exponential; a Lorentzian; and a Gamma function, whose respective spectral tails scale as: $1/\omega^4$; $\exp(-2|\omega|)$; and $1/\omega^{2z}$, where z denotes the shape parameter of the Gamma function. In principle, arbitrarily steep $1/\omega^{3-\alpha}$ scaling can be obtained for $\alpha < 0$ and a Lorentzian pulse function. Scale invariance characterized by exponents $\beta > 2$ is, however, not associated with long-range

correlations.

VII. CONCLUSIONS

A superposition of uncorrelated pulses with durations distributed as $P_\tau(\tau) \sim 1/\tau^\alpha$ displays conditional scale invariance of the frequency power spectral density of the form $1/\omega^\beta$ characterized by $\beta = 3 - \alpha$. This contribution establishes the regimes of validity of the $1/\omega^{3-\alpha}$ scaling. We demonstrate that infinite variance of the pulse durations is necessary for the emergence of self-similar scaling associated with the long-range dependence regime $\beta \in (0, 2)$. This implies a distribution with a divergent upper bound and a finite mean value. Closed-form power spectral density expressions derived for power-law pulse duration distributions with various truncations expose asymptotic self-similar scaling for $1 < \alpha < 3$, and logarithmic corrections to the frequency scaling for $\alpha = 1$ and $\alpha = 3$. Spectral characteristics for $\alpha \notin [1, 3]$ are shown to be determined by the pulse function. Analytically exposed finite-size effects associated with the bounded distribution cutoffs are shown to reduce the frequency range of self-similar scaling by two to three decades. Consequently, spectral scale invariance does not emerge unless the underlying distribution of pulse durations spans at least four logarithmic decades.

We extend the work of van der Ziel, Butz and Milotti by addressing the characteristics of spectral scale invariance in the presence of size limitations for pulse durations. The results presented here are complementary to the work by Lowen and Teich addressing the spectral scale invariance in a Poisson process with a power-law pulse function [11], and in a renewal process with power-law-distributed inter-event times [14]. For a superposition of localized, propagating pulses we demonstrate that power-law distributed durations $P_\tau(\tau) \sim 1/\tau^2$ are equivalent to uniformly distributed velocities, motivating the emergence of power spectral density scaling as $1/f$ without an explicit underlying power-law contribution. The presented model is highly parametrizable in terms of the admitted pulse duration distribution and the pulse function, and it allows for generating synthetic long-range correlation processes with exactly known ranges of scale invariance and explicit power spectral density expressions. It is thus applicable as a framework for testing methods of spectral scaling estimation and identification of the regions of scale invariance.

Appendix A: Origin of power-law scalings

In this appendix it is demonstrated that a power-law distribution of pulse durations readily follows from a superposition of localized and propagating pulses with randomly distributed velocities. This motivates the investigation of power-law-distributed pulse durations as the origin of long-range correlations and power-law scaling of the frequency power spectral density.

1. Motion of localized pulses

The stochastic process given by Eq. (4) describing a superposition of uncorrelated pulses can be extended to include spatial advection along an axis x as

$$\Phi_K(x, t) = \sum_{k=1}^{K(T)} A_k \phi_k(x, t - u_k), \quad (\text{A1})$$

with the pulse function at the arrival time given as

$$\phi_k(x, 0) = \psi\left(\frac{x}{\ell_k}\right), \quad (\text{A2})$$

where ℓ_k is the pulse size. The evolution of each pulse is described by an advection equation

$$\frac{\partial \phi_k}{\partial t} + v_k \frac{\partial \phi_k}{\partial x} = 0, \quad (\text{A3})$$

where v_k is the pulse velocity. The solution of this equation is given by

$$\phi_k(x, t) = \psi\left(\frac{x - v_k t}{\ell_k}\right). \quad (\text{A4})$$

The process defined by Eq. (A1) can accordingly be written as

$$\Phi_K(x, t) = \sum_{k=1}^{K(T)} A_k \psi\left(\frac{x - v_k(t - u_k)}{\ell_k}\right). \quad (\text{A5})$$

At the reference position $x = 0$, this reduces to the process defined by Eq. (4) where $\phi(\theta) = \psi(-\theta)$ and where the duration of each pulse is the transit time $s = \ell/v$. A generalization of this process was used for modelling fluctuations at the boundary of magnetically confined plasmas [47].

When all pulses have the same size ℓ , the probability density of pulse durations $P_s(s)$ is expressed with the probability density of pulse velocities $P_v(v)$ according to the probability of the inverse variable transformation,

$$P_s(s) = \frac{\ell}{s^2} P_v\left(\frac{\ell}{s}\right). \quad (\text{A6})$$

In the following, we consider both bounded and unbounded distributions of pulse velocities giving rise to power-law-distributed pulse durations, and we obtain the closed-form expressions for the resulting frequency power spectral densities.

2. Uniformly distributed velocities

Consider a normalized uniform distribution of pulse velocities

$$\langle v \rangle P_v(v; \sigma) = \begin{cases} \frac{1}{2\sigma} & \text{if } v \in [v_\downarrow, v_\uparrow], \\ 0 & \text{otherwise,} \end{cases} \quad (\text{A7})$$

where $0 < \sigma \leq 1$ is the width of the distribution, and the minimum and the maximum velocities are given respectively as

$$v_\downarrow = \langle v \rangle (1 - \sigma), \quad (\text{A8a})$$

$$v_\uparrow = \langle v \rangle (1 + \sigma). \quad (\text{A8b})$$

From Eq. (A6) it follows that the distribution of pulse durations has a power-law scaling,

$$\langle v \rangle P_s(s; \sigma) = \begin{cases} \frac{1}{2\sigma} \frac{\ell}{s^2} & \text{if } s \in [s_\downarrow, s_\uparrow], \\ 0 & \text{otherwise,} \end{cases} \quad (\text{A9})$$

where the minimum and maximum pulse durations are respectively given by

$$s_\downarrow = \frac{\ell}{v_\uparrow} = \frac{\ell}{\langle v \rangle (1 + \sigma)}, \quad (\text{A10a})$$

$$s_\uparrow = \frac{\ell}{v_\downarrow} = \frac{\ell}{\langle v \rangle (1 - \sigma)}. \quad (\text{A10b})$$

We define Δ to be the logarithmic width of the distribution given by Eq. (A9),

$$\Delta = \frac{s_\uparrow}{s_\downarrow} = \frac{1 + \sigma}{1 - \sigma}. \quad (\text{A11})$$

This definition is aligned with Eq. (30) for the corresponding dimensionless variable. For any given $\Delta > 1$, the width parameter is given by $\sigma = (\Delta - 1)/(\Delta + 1)$, and the average pulse duration then becomes

$$\langle s \rangle = \int_{s_\downarrow}^{s_\uparrow} ds s P_s(s; \sigma) = \frac{\ell}{2\langle v \rangle} \frac{\Delta + 1}{\Delta - 1} \ln \Delta. \quad (\text{A12})$$

This mean value diverges logarithmically in the limit $\Delta \rightarrow \infty$.

In the limit of the widest possible pulse velocity distribution, $\sigma \rightarrow 1$, the minimum velocity vanishes, $v_\downarrow \rightarrow 0$. Arbitrarily slow pulses lead to excessively long pulse durations, and consequently to the divergence of the average pulse duration $\langle s \rangle$ and the maximum duration s_\uparrow , while the minimum duration s_\downarrow remains finite,

$$\lim_{\sigma \rightarrow 1} s_\downarrow = \frac{\ell}{2\langle v \rangle} < \infty, \quad \lim_{\sigma \rightarrow 1} s_\uparrow = \infty, \quad \lim_{\sigma \rightarrow 1} \langle s \rangle = \infty. \quad (\text{A13})$$

As will be discussed presently, this motivates consideration of a lower-truncated Pareto distribution for pulse durations.

3. Pareto distributed durations

Consider now a generalized bounded Pareto distribution of pulse durations with power-law exponent α ,

$$P_s(s; \alpha, s_\downarrow, s_\uparrow) = \begin{cases} \frac{(\alpha - 1)s_\downarrow^{\alpha-1}}{1 - \Delta^{1-\alpha}} s^{-\alpha} & \text{if } s \in [s_\downarrow, s_\uparrow], \\ 0 & \text{otherwise,} \end{cases} \quad (\text{A14})$$

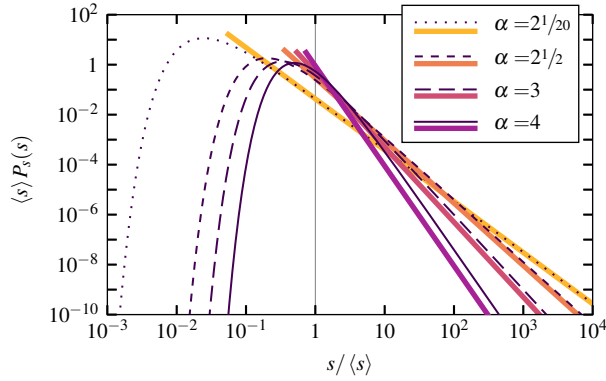


FIG. 4. Probability density functions of the lower-truncated Pareto distribution in Eq. (A17) (thick solid lines) and the inverse Gamma distribution in Eq. (A20) (thin featured lines). The pulse durations are normalized with the mean value $\langle s \rangle$.

whose mean value is given by

$$\langle s \rangle = \frac{(\alpha - 1)(1 - \Delta^{2-\alpha})}{(\alpha - 2)(1 - \Delta^{1-\alpha})} s_{\downarrow}. \quad (\text{A15})$$

When $\alpha = 2$, the Pareto distribution in Eq. (A14) simplifies to the distribution given by Eq. (A9). The corresponding mean value in the limit $\alpha \rightarrow 2$ becomes

$$\lim_{\alpha \rightarrow 2} \langle s \rangle = \frac{\Delta \ln \Delta}{\Delta - 1} s_{\downarrow} = \frac{\ell}{2\langle v \rangle} \frac{\Delta + 1}{\Delta - 1} \ln \Delta, \quad (\text{A16})$$

which coincides with the mean value in Eq. (A12). In Sec. VB it is demonstrated that for $\alpha = 2$ the frequency power spectral density scales as the inverse of the frequency, giving rise to the $1/f$ -noise pattern. This motivates consideration of the generalized bounded Pareto distribution of pulse durations scaling as $P_s(s) \sim 1/s^\alpha$ in the range $s \in [s_{\downarrow}, s_{\uparrow}]$, with a continuous range of exponents α resulting in a range of scaling signatures of the corresponding frequency power spectral density. The details of such a distribution are addressed in Sec. III B.

The limits of the pulse durations in Eq. (A13) for a uniform velocity distribution motivates consideration of the lower-truncated Pareto distribution of pulse durations in the range $s \in [s_{\downarrow}, \infty)$, given by

$$P_s(s; \alpha, s_{\downarrow}) = \begin{cases} (\alpha - 1) s_{\downarrow}^{\alpha-1} s^{-\alpha} & \text{if } s \in [s_{\downarrow}, \infty), \\ 0 & \text{otherwise,} \end{cases} \quad (\text{A17})$$

which is well-defined for $\alpha > 1$. The mean value is finite for $\alpha > 2$ and then given by

$$\langle s \rangle = \frac{\alpha - 1}{\alpha - 2} s_{\downarrow}. \quad (\text{A18})$$

The lower-truncated Pareto distribution for pulse durations is presented in Fig. 4 for various values of the scaling exponent α . Further details on the lower-truncated Pareto distribution in Eq. (A17) and the resulting frequency power spectral density are presented in Appendix B 2.

4. Gamma distributed velocities

Consider now a Gamma distribution of pulse velocities with shape parameter $\alpha - 1$ and scale parameter $\langle v \rangle / (\alpha - 1)$, which for $v > 0$ is given by

$$\langle v \rangle P_v(v; \alpha) = \frac{(\alpha - 1)^\alpha}{\Gamma(\alpha)} \left(\frac{v}{\langle v \rangle} \right)^{\alpha-2} \exp \left(-\frac{(1 - \alpha)v}{\langle v \rangle} \right). \quad (\text{A19})$$

For $\alpha > 2$, this distribution is unimodal and has an exponential tail. For large values of α it resembles a narrow normal distribution, corresponding to the case where all pulses have the same velocity.

According to Eq. (A6), the distribution of pulse durations is in this case given by the inverse Gamma distribution,

$$P_s(s; \alpha) = \frac{\langle v \rangle}{\ell} \frac{(\alpha - 1)^\alpha}{\Gamma(\alpha)} \left(\frac{\ell}{\langle v \rangle s} \right)^\alpha \exp \left(\frac{(1 - \alpha)\ell}{\langle v \rangle s} \right), \quad (\text{A20})$$

with an average pulse duration for $\alpha > 2$ given by

$$\langle s \rangle = \frac{\ell}{\langle v \rangle} \frac{\alpha - 1}{\alpha - 2}. \quad (\text{A21})$$

This is equivalent to the mean value in Eq. (A18) for the lower-truncated Pareto distribution, up to the α -independent prefactor.

At relatively high values of s , the inverse Gamma distribution in Eq. (A20) follows the same power-law scaling $P_s(s) \sim s^{-\alpha}$ as the lower-truncated Pareto distribution in Eq. (A17). Figure 4 reveals the parallel tails of the corresponding distributions for several values of α . The difference with respect to the lower-truncated Pareto distribution is that the inverse Gamma distribution is defined on the entire positive range $s \in (0, \infty)$, without a cutoff at s_{\downarrow} . Instead, it has a relatively sharp but smooth drop at low values of s , as demonstrated in Fig. 4. A gradual cutoff may be considered more representative of physical finite-size power-law scaling than the abrupt cutoff of the lower-truncated Pareto distribution given by Eq. (A17). Further details on the inverse Gamma distribution for pulse durations and the resulting frequency power spectral density are presented in Appendix B 3.

Appendix B: Power spectral densities for alternative power-law distributions of pulse durations

This appendix is an extension of Secs. III and V. It presents the definitions of the remaining variants of power-law distributions, complementary to Sec. III B, followed by the derivation and analysis of the associated power spectral densities, complementary to Sec. V B.

1. Upper-truncated Pareto distribution

The Pareto distribution defined by Eq. (28) with an upper-truncated support $\tau \in (0, \tau_{\uparrow}]$ is well-defined for $\alpha < 1$. Applying conditions (26) and (27) yields the following parameters

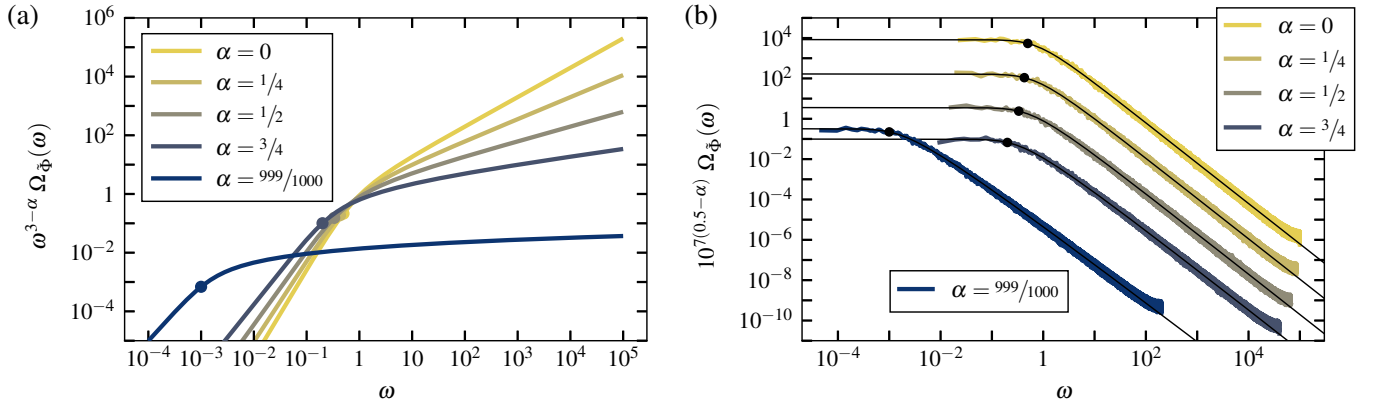


FIG. 5. Power spectral densities for a super-position of one-sided exponential pulses with upper-truncated-Pareto distributed durations. Filled circles mark the cutoff frequencies $\omega\tau_{\uparrow} = 1$. The presented values of α span the entire range where the distribution is well-defined. (a) Compensated analytical power spectral densities $\omega^{3-\alpha} \Omega_{\Phi}(\omega; \alpha)$ with Ω_{Φ} given by Eq. (B4). (b) Empirical power spectral densities for realizations of the process. The respective analytical power spectral densities are plotted with solid black curves. Vertical shifting by α -dependent factors is applied to avoid overlapping.

of the distribution,

$$\eta(\alpha, \tau_{\uparrow}) = -(\alpha - 1) \tau_{\uparrow}^{\alpha-1}, \quad (\text{B1})$$

$$\tau_{\uparrow}(\alpha) = \frac{\alpha - 2}{\alpha - 1}. \quad (\text{B2})$$

The pulse duration variance is finite for $\alpha < 1$ and then given by

$$\langle \tau^2 \rangle(\alpha) = \frac{\alpha - 2}{\alpha - 3} \tau_{\uparrow}. \quad (\text{B3})$$

The upper-truncated Pareto distribution was not motivated in Appendix A.

For the upper-truncated Pareto distribution characterized by Eqs. (28) and (B1)–(B2), the power spectral density given by Eq. (24) for $0 < \alpha < 1$ becomes

$$\Omega_{\Phi}(\omega; \alpha) = \frac{2(\alpha - 2)}{(\alpha - 3)} {}_2F_1\left(1, \frac{3 - \alpha}{2}, \frac{5 - \alpha}{2}; -\tau_{\uparrow}^2 \omega^2\right) \tau_{\uparrow}, \quad (\text{B4})$$

where τ_{\uparrow} is given by Eq. (B2) and ${}_2F_1$ is a hypergeometric function defined by Gauss series [48]. As discussed in Sec. IV, spectral scale invariance is expected only in the limit $\alpha \rightarrow 1^-$, in which case the asymptotic Lorentzian tail $\sim 1/\omega^2$ results from the discontinuity in the pulse function rather than from self-similarity of the process. The lack of self-similar scaling is confirmed in Fig. 5(a), which shows that the power spectral density given by Eq. (B4) compensated by a factor $\omega^{3-\alpha}$ does not maintain a constant value in any frequency range. Hence, $\Omega_{\Phi} \approx 1/\omega^{3-\alpha}$ for $0 < \alpha < 1$. Figure 5(b) presents the empirical power spectral densities obtained for realizations of the process for $\gamma = 10$. The normalized sampling and duration intervals are given by $\tau_{\uparrow}/(4 \times 10^5)$ and $640\tau_{\uparrow}$, respectively. The empirical results demonstrate perfect agreement with the corresponding analytical predictions, and show that a Lorentzian shape is obtained irrespectively of the value of α .

2. Lower-truncated Pareto distribution

The Pareto distribution defined by Eq. (28) with a lower-truncated support $\tau \in [\tau_{\downarrow}, \infty)$ is well-defined for $\alpha > 2$. This corresponds to the standard Pareto distribution. Applying conditions (26) and (27) yields the following parameters of the distribution,

$$\eta(\alpha, \tau_{\downarrow}) = (\alpha - 1) \tau_{\downarrow}^{\alpha-1}, \quad (\text{B5})$$

$$\tau_{\downarrow}(\alpha) = \frac{\alpha - 2}{\alpha - 1}. \quad (\text{B6})$$

The pulse duration variance is finite for $\alpha > 3$ and then given by

$$\langle \tau^2 \rangle(\alpha) = \frac{\alpha - 2}{\alpha - 3} \tau_{\downarrow}. \quad (\text{B7})$$

This definition of the lower-truncated Pareto distribution is aligned with Eq. (A17) motivated in Appendix A.2.

For the lower-truncated Pareto distribution characterized by Eqs. (28) and (B5)–(B6), the power spectral density given by Eq. (24) for $\alpha > 2$ becomes

$$\Omega_{\Phi}(\omega; \alpha) = \frac{2}{\omega^2} {}_2F_1\left(1, \frac{\alpha - 1}{2}, \frac{\alpha + 1}{2}; \frac{-1}{\tau_{\downarrow}^2 \omega^2}\right), \quad (\text{B8})$$

where τ_{\downarrow} is given by Eq. (B6). Spectral scale invariance is expected for $2 < \alpha \leq 3$. Compensating Eq. (B8) by $\omega^{3-\alpha}$ exposes self-similar scaling in the low-frequency limit,

$$\lim_{\omega \rightarrow 0} \Omega_{\Phi}(\omega; 2^{1/4}) |\omega|^{3/4} \frac{2}{\pi} (30 + 20\sqrt{2})^{1/4} = 1, \quad (\text{B9a})$$

$$\lim_{\omega \rightarrow 0} \Omega_{\Phi}(\omega; 2^{1/2}) |\omega|^{1/2} \frac{\sqrt{6}}{\pi} = 1, \quad (\text{B9b})$$

$$\lim_{\omega \rightarrow 0} \Omega_{\Phi}(\omega; 2^{3/4}) |\omega|^{1/4} \frac{2}{3\pi} \left(\frac{7}{3}\right)^{3/4} \left(1 + \frac{1}{\sqrt{2}}\right)^{-1/2} = 1. \quad (\text{B9c})$$

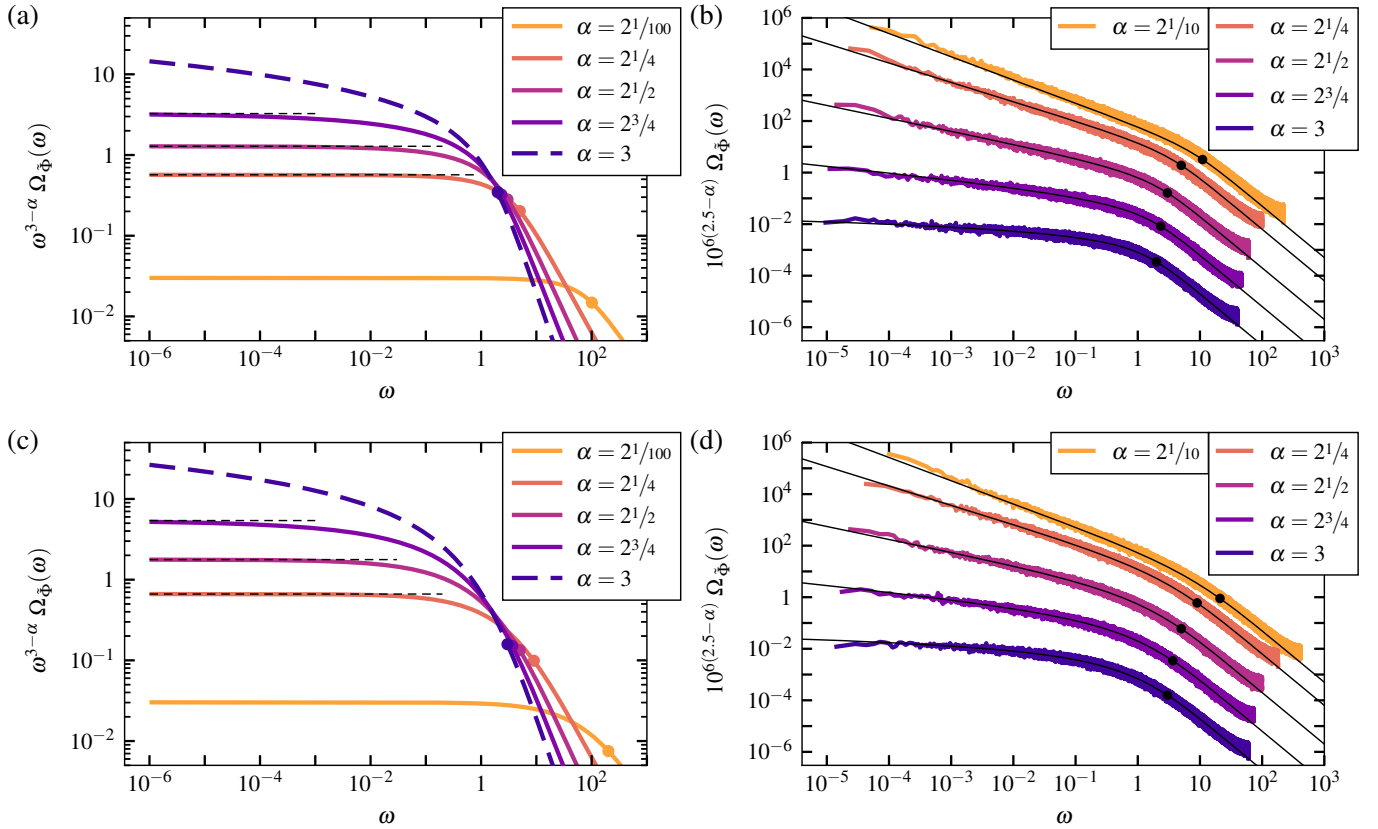


FIG. 6. Power spectral densities for a super-position of one-sided exponential pulses with distributed durations: (top row) lower-truncated Pareto distribution with the cutoff frequency $\omega\tau_{\downarrow} = 1$; (bottom row) inverse Gamma distribution with the cutoff frequency $\omega\tau_m = 1$. Explanation of symbols as in Fig. 3. Left column: Compensated analytical power spectral densities $\omega^{3-\alpha}\Omega_{\Phi}(\omega; \alpha)$ with Ω_{Φ} given by: (a) Eq. (B8); (c) Eq. (B14), with ω -independent factors in: (a) Eqs. (B9); (c) Eqs. (B15a)–(B15c). Right column: Empirical power spectral densities for realizations of the process. The respective analytical power spectral densities are plotted with solid black curves. Vertical shifting by α -dependent factors is applied to avoid overlapping.

The inverse of the ω -independent compensating factors in Eqs. (B9) indicate the levels to which the compensated power spectral density tends asymptotically in the low-frequency limit. These levels are marked in Fig. 6(a) with horizontal dashed black lines. The frequency ranges where the compensated-spectra curves overlap with the constant-level lines indicate regions of $1/\omega^{3-\alpha}$ scaling. Figure 6(a) demonstrates also that the compensated spectra for $\alpha \rightarrow 2^+$ manifest a clear signature of scale invariance [49].

For $\alpha = 3$ the power spectral density in Eq. (B8) simplifies to

$$\Omega_{\Phi}(\omega; 3) = \frac{1}{2} \ln \left(1 + \frac{4}{\omega^2} \right), \quad (\text{B10})$$

revealing logarithmic corrections to the frequency scaling. The compensated spectra in Fig. 6(a) confirm the lack of self-similar scaling for $\alpha = 3$. The corresponding empirical power spectral densities presented in Fig. 6(b) are aligned with the analytical expressions. The underlying process realizations are obtained for $\gamma = 10$. The normalized sampling and duration intervals are given by $\tau_{\downarrow}/40$ and $64 \times 10^5 \tau_{\downarrow}$, respectively.

3. Inverse Gamma distribution

The inverse Gamma distribution for the normalized pulse durations follows from Eq. (A20). It is well-defined for $\alpha > 2$ and then given by

$$P_{\tau}(\tau; \alpha) = \frac{(\alpha - 2)^{\alpha-1}}{\Gamma(\alpha - 1)} \tau^{-\alpha} \exp \left(\frac{2 - \alpha}{\tau} \right). \quad (\text{B11})$$

This distribution has a mode at

$$\tau_m = \frac{\alpha - 2}{\alpha}, \quad (\text{B12})$$

which marks the onset of the smooth exponential decrease to zero value in the limit $\tau \rightarrow 0$, as shown in Fig. 4.

The parametrization $P_{\tau}(\tau; \alpha)$ of the inverse Gamma distribution in Eq. (B11) aligns it to the power-law notation $\tau^{-\alpha}$ used for the Pareto distributions introduced in Sec. III A. The inverse Gamma distribution has the same support span $\tau \in (0, \infty)$ as the ill-defined unbounded Pareto distribution. However, due to the smooth cutoff at low values of τ resulting from the exponential term, it is both well-defined according to

Eq. (26), and it has a finite, non-diverging mean satisfying the normalization condition (27).

As highlighted in Appendix A4, the inverse Gamma distribution is qualitatively comparable to the lower-truncated Pareto distribution: it has the same scaling for the tail, effectively a cutoff at low pulse durations, and a finite pulse duration variance for $\alpha > 3$, which for the inverse Gamma distribution is given by

$$\langle \tau^2 \rangle(\alpha) = \frac{\alpha - 2}{\alpha - 3}. \quad (\text{B13})$$

The power spectral density in Eq. (24) is for the inverse Gamma distribution in Eq. (B11) with $\alpha > 2$ given by

$$\Omega_{\tilde{\Phi}}(\omega; \alpha) = \begin{cases} \frac{\sin(|\omega|) [\pi - 2 \text{Si}(|\omega|)] - 2 \cos(\omega) \text{Ci}(|\omega|)}{\Gamma(\alpha-1)} \left[|\omega|^{\alpha-3} \cos\left(\frac{\pi(\alpha-1)}{2}\right) + (\alpha-2)|\omega| \right. \\ \quad \times \pi(\alpha-2)^{\alpha-1} \csc(\pi(\alpha-1)) \\ \quad \left. + {}_pF_q\left(1, \left\{\frac{4-\alpha}{2}, \frac{5-\alpha}{2}\right\}, \frac{(\alpha-2)^2}{-4} \omega^2\right) \right] & \text{if } \alpha = 3, \\ \times (\alpha-2)^2 \Gamma(\alpha-3) & \text{otherwise,} \end{cases} \quad (\text{B14})$$

where $\text{Si}(z) = \int_0^z dt \sin(t)/t$ and $\text{Ci}(z) = -\int_z^\infty dt \cos(t)/t$ are sine and cosine integrals, respectively, and ${}_pF_q$ is a generalized hypergeometric function defined by generalized hypergeometric series [50]. Compensating Eq. (B14) by $\omega^{3-\alpha}$ reveals

the expected scaling in the low-frequency limit,

$$\lim_{\omega \rightarrow 0} \Omega_{\tilde{\Phi}}(\omega; 2^{1/4}) |\omega|^{3/4} \frac{2 \Gamma(\frac{5}{4})}{\pi \sin(\frac{\pi}{8})} = 1, \quad (\text{B15a})$$

$$\lim_{\omega \rightarrow 0} \Omega_{\tilde{\Phi}}(\omega; 2^{1/2}) |\omega|^{1/2} \frac{1}{\sqrt{\pi}} = 1, \quad (\text{B15b})$$

$$\lim_{\omega \rightarrow 0} \Omega_{\tilde{\Phi}}(\omega; 2^{3/4}) |\omega|^{1/4} \frac{4\sqrt{2} \Gamma(\frac{7}{4})}{\pi 3^{7/4} \sqrt{1 + \frac{1}{\sqrt{2}}}} = 1, \quad (\text{B15c})$$

$$\lim_{\omega \rightarrow 0} \Omega_{\tilde{\Phi}}(\omega; 3) \left[\ln \left(1 + \frac{4}{\omega^2} \right) \right]^{-1} = 1. \quad (\text{B15d})$$

For $\alpha = 3$ the same logarithmic correction to the frequency scaling is present as for the power spectral densities in Eqs. (B10) and (47e) derived for the lower-truncated Pareto and the bounded Pareto distributions, respectively. For $\alpha = 2$ the inverse Gamma distribution vanishes and so does the power spectral density given by Eq. (B14).

Figure 6(c) confirms the presence of the $1/\omega^{3-\alpha}$ scaling for $2 < \alpha < 3$, and the lack thereof for $\alpha = 3$. Figure 6(d) shows the empirical power spectral densities obtained for realizations of the process for $\gamma = 10$. The normalized sampling and duration intervals are given by $\tau_m/40$ and $64 \times 10^5 \tau_m$, respectively. Expectedly, the empirical results match the analytical expressions. Figure 6 demonstrates also that the scaling signatures of the frequency power spectral density obtained for the corresponding values of α are remarkably similar between the inverse Gamma distribution with a smooth cutoff at τ_m , and the lower-truncated Pareto distribution with an abrupt cutoff at τ_\downarrow .

ACKNOWLEDGMENTS

This work was supported by the UiT Aurora Centre Program, UiT The Arctic University of Norway (2020). Discussions with Martin Rypdal and Audun Theodorsen are gratefully appreciated.

-
- [1] G. Boffetta, V. Carbone, P. Giuliani, P. Veltri, and A. Vulpiani, Power laws in solar flares: Self-organized criticality or turbulence?, *Phys. Rev. Lett.* **83**, 4662 (1999).
 - [2] T. Chang, Self-Organized Criticality, Multi-Fractal Spectra, and Intermittent Merging of Coherent Structures in the Magnetotail, *Astrophys. Space Sci.* **264**, 303 (1999).
 - [3] P. Veltri, MHD turbulence in the solar wind: self-similarity, intermittency and coherent structures, *Plasma Physics and Controlled Fusion* **41**, A787 (1999).
 - [4] L. de Arcangelis, C. Godano, E. Lippiello, and M. Nicodemi, Universality in solar flare and earthquake occurrence, *Phys. Rev. Lett.* **96**, 051102 (2006).
 - [5] V. M. Uritsky, M. Paczuski, J. M. Davila, and S. I. Jones, Coexistence of self-organized criticality and intermittent turbulence in the solar corona, *Phys. Rev. Lett.* **99**, 025001 (2007).
 - [6] K. Kiyani, S. C. Chapman, B. Hnat, and R. M. Nicol, Self-similar signature of the active solar corona within the inertial range of solar-wind turbulence, *Phys. Rev. Lett.* **98**, 211101 (2007).
 - [7] M. J. Aschwanden, Self-organized criticality in solar and stellar flares: Are extreme events scale-free?, *The Astrophysical Journal* **880**, 105 (2019).
 - [8] M. J. Aschwanden and T. D. de Wit, Correlation of the sunspot number and the waiting-time distribution of solar flares, coronal mass ejections, and solar wind switchback events observed with the Parker Solar Probe, *The Astrophysical Journal* **912**, 94 (2021).
 - [9] M. Pereira, C. Gissinger, and S. Fauve, $1/f$ noise and long-term memory of coherent structures in a turbulent shear flow, *Phys. Rev. E* **99**, 023106 (2019).
 - [10] H. Pécseli, *Fluctuations in Physical Systems* (Cambridge University Press, 2000).
 - [11] S. Lowen and M. Teich, *Fractal-Based Point Processes* (Wiley, Hoboken, NJ, 2005) Chap. 9.
 - [12] M. J. Aschwanden, *Self-Organized Criticality in Astrophysics*, Vol. 11 (Springer Berlin, Heidelberg, 2011) Chap. 4.8, pp. 129–

- 135.
- [13] G. Samorodnitsky, *Stochastic Processes and Long Range Dependence* (Springer, 2016) Chap. 3.4.
- [14] S. B. Lowen and M. C. Teich, Fractal renewal processes generate $1/f$ noise, *Phys. Rev. E* **47**, 992 (1993).
- [15] B. Kaulakys, V. Gontis, and M. Alaburda, Point process model of $1/f$ noise vs a sum of Lorentzians, *Phys. Rev. E* **71**, 051105 (2005).
- [16] L. Silvestri, L. Fronzoni, P. Grigolini, and P. Allegrini, Event-driven power-law relaxation in weak turbulence, *Phys. Rev. Lett.* **102**, 014502 (2009).
- [17] N. Leibovich, A. Dechant, E. Lutz, and E. Barkai, Aging Wiener-Khinchin theorem and critical exponents of $1/f^\beta$ noise, *Phys. Rev. E* **94**, 052130 (2016).
- [18] E. Milotti, Exact numerical simulation of power-law noises, *Phys. Rev. E* **72**, 056701 (2005).
- [19] A. van der Ziel, On the noise spectra of semi-conductor noise and of flicker effect, *Physica* **16**, 359 (1950).
- [20] A. R. Butz, A theory of $1/f$ noise, *J. Stat. Phys.* **4**, 199–216 (1972).
- [21] A. Kononovicius and B. Kaulakys, $1/f$ noise from the sequence of nonoverlapping rectangular pulses, *Phys. Rev. E* **107**, 034117 (2023).
- [22] B. N. Costanzi and E. D. Dahlberg, Emergent $1/f$ noise in ensembles of random telegraph noise oscillators, *Phys. Rev. Lett.* **119**, 097201 (2017).
- [23] H. J. Jensen, *Self-Organized Criticality: Emergent Complex Behavior in Physical and Biological Systems* (Cambridge Lecture Notes in Physics (Cambridge University Press, 1998).
- [24] J. Bernamont and M. Bernamont, Fluctuations de potentiel aux bornes d'un conducteur métallique de faible volume parcouru par un courant, *Ann. Phys.* **11**, 71 (1937).
- [25] D. M. Fleetwood, *Noise in Nanoscale Semiconductor Devices*, edited by T. Grassler (Springer International Publishing, Cham, 2020) pp. 1–31.
- [26] D. M. Fleetwood, Low-frequency noise in nanowires, *Nanoscale* **15**, 12175 (2023).
- [27] O. E. Garcia and A. Theodorsen, Auto-correlation function and frequency spectrum due to a super-position of uncorrelated exponential pulses, *Phys. Plasmas* **24**, 032309 (2017).
- [28] N. Campbell, The study of discontinuous phenomena, *Proc. Cambridge Philos. Soc.* **15**, 117 (1909).
- [29] S. O. Rice, Mathematical analysis of random noise, *Bell System Technical Journal* **23**, 282 (1944).
- [30] O. E. Garcia, R. Kube, A. Theodorsen, and H. L. Pécseli, Stochastic modelling of intermittent fluctuations in the scrape-off layer: Correlations, distributions, level crossings, and moment estimation, *Phys. Plasmas* **23**, 052308 (2016).
- [31] M. A. Korzeniowska, A. Theodorsen, M. Rypdal, and O. E. Garcia, Apparent universality of $1/f$ spectra as an artifact of finite-size effects, *Phys. Rev. Res.* **5**, L022066 (2023).
- [32] F. Hooge, $1/f$ noise sources, *IEEE Transactions on Electron Devices* **41**, 1926 (1994).
- [33] F. Hooge and P. Bobbert, On the correlation function of $1/f$ noise, *Physica B: Condensed Matter* **239**, 223 (1997).
- [34] W. Schottky, Small-shot effect and flicker effect, *Phys. Rev.* **28**, 74 (1926).
- [35] J. B. Johnson, The Schottky effect in low frequency circuits, *Phys. Rev.* **26**, 71 (1925).
- [36] A. van der Ziel, Flicker noise in electronic devices, *Advances in Electronics and Electron Physics* **49**, 225 (1979).
- [37] F. K. Du Pré, A suggestion regarding the spectral density of flicker noise, *Phys. Rev.* **78**, 615 (1950).
- [38] H. C. Montgomery, Electrical noise in semiconductors, *Bell System Technical Journal* **31**, 950 (1952), <https://onlinelibrary.wiley.com/doi/pdf/10.1002/j.1538-7305.1952.tb01415.x>.
- [39] R. L. Petritz, On the theory of noise in p-n junctions and related devices, *Proceedings of the IRE* **40**, 1440 (1952).
- [40] R. H. Kingston, ed., *Semiconductor Surface Physics* (University of Pennsylvania Press, Philadelphia, 1957).
- [41] M. Niemann, H. Kantz, and E. Barkai, Fluctuations of $1/f$ noise and the low-frequency cutoff paradox, *Phys. Rev. Lett.* **110**, 140603 (2013).
- [42] M. A. Rodríguez, Class of perfect $1/f$ noise and the low-frequency cutoff paradox, *Phys. Rev. E* **92**, 012112 (2015).
- [43] S. Sadegh, E. Barkai, and D. Krapf, $1/f$ noise for intermittent quantum dots exhibits non-stationarity and critical exponents, *New Journal of Physics* **16**, 113054 (2014).
- [44] R. Kenna, D. A. Johnston, and W. Janke, Scaling relations for logarithmic corrections, *Phys. Rev. Lett.* **96**, 115701 (2006).
- [45] A. W. Sandvik, Continuous quantum phase transition between an antiferromagnet and a valence-bond solid in two dimensions: Evidence for logarithmic corrections to scaling, *Physical Review Letters* **104**, 075701 (2010).
- [46] S. Hong and D.-H. Kim, Logarithmic finite-size scaling correction to the leading Fisher zeros in the p -state clock model: A higher-order tensor renormalization group study, *Phys. Rev. E* **101**, 012124 (2020).
- [47] J. M. Losada, A. Theodorsen, and O. E. Garcia, Stochastic modeling of blob-like plasma filaments in the scrape-off layer: Theoretical foundation, *Physics of Plasmas* **30**, 042518 (2023).
- [48] A. B. Olde Daalhuis, NIST Digital Library of Mathematical Functions, Hypergeometric Function, Release 1.1.9 (2022), Chap. 15, <https://dlmf.nist.gov/15.2.E1>.
- [49] For $1 < \alpha \leq 2$ the mean value for the dimensional lower-truncated Pareto distribution is infinite, $\langle s \rangle = \infty$, preventing the normalization of the power spectral density into the form given by Eq. (24). Nevertheless, the dimensional power spectral density integral in Eq. (20) can be solved for a generic lower-truncated Pareto distribution defined on a support $s \in [s_\downarrow, \infty)$ as $P_s(s) = \eta s^{-2}$,
- $$\int_{s_\downarrow}^{\infty} ds s^2 P_s(s) \varrho_\phi(so) = \eta \left(\frac{\pi}{|o|} - \frac{2 \arctan(oso_\downarrow)}{o} \right), \quad (\text{B16})$$
- which in the limit $s_\downarrow \rightarrow 0$ integrates to $\eta\pi/|o|$, revealing the expected $1/o$ scaling, in line with the $\beta = 3 - \alpha$ relation for $\alpha = 2$.
- [50] R. A. Askey and A. B. Olde Daalhuis, NIST Digital Library of Mathematical Functions, Generalized Hypergeometric Functions and Meijer G-Function, Release 1.1.9 (2022), Chap. 16, <https://dlmf.nist.gov/16.2.E1>.